Bone 88 (2016) 74–84

Contents lists available at ScienceDirect

Bone

journal homepage: www.elsevier.com/locate/bone

Full Length Article

Loss of BMP signaling through BMPR1A in osteoblasts leads to greater collagen cross-link maturation and material-level mechanical properties in mouse femoral trabecular compartments

Yanshuai Zhang [a], Erin Gatenby McNerny [b], Masahiko Terajima [d], Mekhala Raghavan [c], Genevieve Romanowicz [a], Zhanpeng Zhang [a], Honghao Zhang [a], Nobuhiro Kamiya [a,e,g,h], Margaret Tantillo [a], Peizhi Zhu [c], Gregory J. Scott [f], Manas K. Ray [f], Michelle Lynch [i], Peter X. Ma [a], Michael D. Morris [c], Mitsuo Yamauchi [d], David H. Kohn [a,b], Yuji Mishina [a,e,f,*]

[a] Department of Biologic and Materials Sciences, School of Dentistry, University of Michigan, MI, USA
[b] Biomedical Engineering, College of Engineering, University of Michigan, MI, USA
[c] Department of Chemistry, College of Literature, Science and the Arts, University of Michigan, MI, USA
[d] School of Dentistry, University of North Carolina at Chapel Hill, North Carolina, NC, USA
[e] Reproductive and Developmental Biology Laboratory, National Institute of Environmental Health Sciences, National Institutes of Health, Research Triangle Park, NC 27709, USA
[f] Knock Out Core, National Institute of Environmental Health Sciences, National Institutes of Health, Research Triangle Park, NC 27709, USA
[g] Center for Excellence in Hip Disorders, Texas Scottish Rite Hospital for Children, Dallas, TX 75219, USA
[h] Faculty of Budo and Sport Studies, Tenri University, Nara, Japan
[i] Office of Research, School of Dentistry, University of Michigan, MI, USA

ARTICLE INFO

Article history:
Received 5 April 2014
Revised 26 March 2016
Accepted 22 April 2016
Available online 23 April 2016

Keywords:
BMP receptor type 1A
Collagen cross-links
Cortical geometry
Bone quality
Biomechanical properties

ABSTRACT

Bone morphogenetic protein (BMP) signaling pathways play critical roles in skeletal development and new bone formation. Our previous study, however, showed a negative impact of BMP signaling on bone mass because of the osteoblast-specific loss of a BMP receptor (i.e. BMPR1A) showing increased trabecular bone volume and mineral density in mice. Here, we investigated the bone quality and biomechanical properties of the higher bone mass associated with BMPR1A deficiency using the osteoblast-specific *Bmpr1a* conditional knockout (cKO) mouse model. Collagen biochemical analysis revealed greater levels of the mature cross-link pyridinoline in the cKO bones, in parallel with upregulation of collagen modifying enzymes. Raman spectroscopy distinguished increases in the mature to immature cross-link ratio and mineral to matrix ratio in the trabecular compartments of cKO femora, but not in the cortical compartments. The mineral crystallinity was unchanged in the cKO in either the trabecular or cortical compartments. Further, we tested the intrinsic material properties by nanoindentation and found significantly higher hardness and elastic modulus in the cKO trabecular compartments, but not in the cortical compartments. Four point bending tests of cortical compartments showed lower structural biomechanical properties (i.e. strength and stiffness) in the cKO bones due to the smaller cortical areas. However, there were no significant differences in biomechanical performance at the material level, which was consistent with the nanoindentation test results on the cortical compartment. These studies emphasize the pivotal role of BMPR1A in the determination of bone quality and mechanical integrity under physiological conditions, with different impact on femoral cortical and trabecular compartments.

1. Introduction

Bone morphogenetic proteins (BMPs) were originally described as secreted substances that can induce ectopic bone formation when implanted subcutaneously [1]. Since then, the osteogenic function of BMPs has been extensively examined, mainly using in vitro tissue cultured systems [2]. Since the FDA approved the use of BMP2 and BMP7 in clinical settings for long bone open fractures, nonunion fractures and spinal fusion, the impact of BMPs during fracture healing has been extensively studied [3]. However, the impact of BMP signaling in bone homeostasis in a physiological setting has been relatively neglected due to the lack of appropriate in-vivo model systems.

BMP signals are mediated by type I and type II serine/threonine kinase receptors. Three type I receptors for BMPs (BMPR1A or ALK3,

* Corresponding author at: Department of Biologic and Materials Sciences, School of Dentistry, University of Michigan, 1011 N. University Ave., Ann Arbor, MI 48109, USA.
E-mail address: mishina@umich.edu (Y. Mishina).

http://dx.doi.org/10.1016/j.bone.2016.04.022
8756-3282/

BMPR1B or ALK6, and ACVR1 or ALK2) have been identified and characterized [4]. BMPR1A is ubiquitously expressed in most types of cells, including osteoblasts. We and others have demonstrated the pleiotropic functions of BMP signaling mediated by BMPR1A using a conditional mutant allele for *Bmpr1a* [5]. Our recent study found that disruption of *Bmpr1a* in an osteoblast-specific manner leads to an increase of trabecular bone mass in the femora, spine and ribs [6–9], contrary to what was expected based on the osteoinductive functions of BMPs [10,11]. We found a lower bone formation rate in trabecular compartments of the mutant mice [7,8]. However, we also found that disruption of *Bmpr1a* in osteoblasts severely compromises osteoclastogenesis through alterations in the Wnt-RANKL axis, which subsequently results in the increase in bone mass. We also reported that an osteoblast-specific knockout of another type I receptor for BMPs, *Acvr1*, leads to nearly identical phenotypes as *Bmpr1a* cKO mice, with increases of bone mass in many, but not all, of the bones [12]. Most recently, it is reported that suppression of BMP signaling by administration of a soluble form of a BMPR1A fusion protein in wild-type mice also leads to an increase in bone mass [13]. In the cases of gain-of-function of BMP4 mouse models, bone mass is reduced [14], while loss-of-function of BMP2 results in reduced bone mass [10,11]. Taken together, these results suggest that the functions of BMPs on bone homeostasis are more complicated than what was earlier believed; i.e. BMP signaling in osteoblasts activates both osteoblast anabolic function and catabolic function through enhancing osteoclastogenesis [2]. In the case of the osteoblast-specific knockout of *Bmp1a* and *Acvr1*, the balance moves to further reduction of catabolic function, leading to an increase of trabecular bone mass [7,8,12]. The subsequently important question is whether the higher bone mass found in the cKO mice leads to increases in bone quality and mechanical properties.

Bone mineral density (BMD) has been traditionally used clinically to evaluate bone mass as a surrogate for bone strength. However, BMD does not always predict fracture risk [15] and it is now well accepted that both bone quality and bone mass are important factors in determining bone strength [16]. Bone quality affects biomechanical properties differentially depending on the amount and structure of bone matrix (i.e. mineral and collagen fiber) [17]. Bone matrices consist primarily of inorganic mineral and organic fibrillar collagen. The amount and structure of both the mineral and matrix components contribute to biomechanical properties of bone, though mineral contributes more to stiffness whereas collagen contributes more to flexibility [18]. Bone strength at the material level (aka tissue level) may be determined by the degree of mineralization, collagen properties and the way these two components are organized [17].

Covalent intermolecular collagen cross-linking, the final process of collagen biosynthesis, is important for the stability of collagen fibrils and to organize mineralization [19]. Collagen cross-linking can be divided into two categories, namely, enzymatic and non-enzymatic cross-linking. In bone, enzymatic cross-links are considered to be beneficial because they have a positive effect on the mechanical properties of bone, within a certain range [20]. Enzymatic collagen cross-linking is initiated by the conversion of telopeptidyl lysine (Lys) or hydroxylysine (Hyl) residues to the respective aldehydes by the action of lysyl oxidase (LOX) and, possibly LOX-like proteins (LOXLs) [20]. The aldehydes produced then condense with the juxtaposed ε-amino group of Lys or Hyl on a neighboring molecule to form divalent cross-links, which can then spontaneously mature into trivalent cross-links [21]. The major divalent cross-links in bone collagen are dehydrodihydroxylysinonorleucine/its ketoamine (deH-DHLNL) and dehydrohydroxylysinonorleucine/its ketoamine (deH-HLNL), and trivalent cross-links, Lysyl Pyridinoline (LP) and Hydroxylysyl Pyridinoline (HP) and pyrrole. The pathway of cross-linking is mainly determined by the extent of Lys hydroxylation, a post-translational modification catalyzed by lysyl hydroxylases (LHs) encoded by procollagen lysine, 2-oxoglutarate 5-dioxygenase, *Plods*.

Understanding the quality and biomechanical properties of the higher bone mass induced by loss of BMPR1A is necessary for developing clinical treatments based on BMP signaling. Here, we report for the first time that BMP signaling through BMPR1A in osteoblasts plays a critical role in maintaining bone quality, including collagen cross-links and mineralization. Loss of BMPR1A signaling in osteoblasts affected bone material quality in femoral cortical and trabecular compartments differently, which led to alterations in biomechanical properties of femoral bones. Our results uncover novel aspects of BMP signaling in biomechanics, bone quality, and bone mass.

2. Materials and methods

2.1. Animals

Transgenic mice expressing the tamoxifen (TM)-inducible Cre fusion protein Cre-ER™ [22] under the control of a 3.2 kb mouse pro-collagen *a*(*I*) promoter [23] (*Col1-CreER*™) were generated by pronuclear injection and crossed with floxed *Bmpr1a* mice [24]. These mice were maintained in a 129S6 and C57BL6/J mixed background. TM (150 mg/kg) was gavaged to males twice a week from 16 to 20 weeks of age and tissues were collected at week 22 (n = 12 per group). The resulting mice developed similar bone phenotypes as we previously reported [8], including an increase in trabecular thickness and tissue mineral density in femoral trabecular compartments (Supplementary Table 1) and alterations in expression of marker genes for osteoblasts and osteoclasts (data not shown). However, unlike our previous report that shows a slight decrease of tissue mineral density in femoral cortical compartments, no such changes were found in this parameter (Supplementary Table 2), presumably due to the shorter period of TM treatment.

Femora and 6th ribs were isolated; muscles were removed, and bones were wrapped with Ca-PBS soaked gauze and stored at −80 °C until use. Right femora were used for collagen analyses, Raman microscopy and nanoindentation. Left femora were scanned for micro computed tomography (μCT) followed by 4-point bending tests. Ribs were used for nanoindentation to confirm the findings in the femora. Tibiae were immediately flushed to remove bone marrow at the time of dissection and used for RNA extraction. Results were analyzed by comparing *Bmpr1a* cKO (*Col1-CreER*(+):*Bmpr1a fx/fx*, cKO, hereafter) and littermate controls (*Col1-CreER*(−): *Bmpr1a fx/fx*, control, hereafter) that also received TM. No side effects on bone morphology and body weight were observed using this TM regimen [8]. The animal protocol was approved by the Institutional Animal Care and Use Committees at National Institute of Environmental Health Sciences and University of Michigan.

2.2. Amino acid analysis

The right femora (n = 6 each group) were removed and soft tissues were cleaned off the bone surface. Bone marrow was removed by flushing with cold PBS and then the samples, including both cortical and trabecular compartments, were pulverized to a fine powder under liquid N2 using a Spex Freezer Mill (Spex Metuchen, NJ, USA). Pulverized samples were washed with cold PBS and then with cold distilled water several times by repeated centrifugation (4000 *g*), and lyophilized. 1 mg of dried sample was hydrolyzed with 6 N HCl and an aliquot of hydrolysate was subjected to amino acid analysis on a Varian high performance liquid chromatography system (Prostar 240/310, Varian, Walnut Creek, CA, USA) with a strong cation exchange column (AA-911, Transgenomic, San Jose, CA, USA) [25]. Based on the hydroxyproline (Hyp) value, the collagen content was calculated and expressed as μg/mg of dried sample. The extent of Lys hydroxylation of collagen was calculated by the Hyl residues per 300 residues of Hyp and expressed as mol/mol of collagen [26].

2.3. Collagen cross-link analysis

An aliquot of whole bone sample used for amino acid analysis was demineralized with 0.5 M EDTA, 0.05 M Tris–HCl, pH 7.4, for 2 weeks, washed with cold distilled water exhaustively and lyophilized. 2 mg of

demineralized collagen was then suspended, reduced with standardized NaB^3H_4 [27], and hydrolyzed with 6 N HCl as described above. An aliquot of hydrolysate was subjected to amino acid analysis to determine Hyp and then the hydrolysate with known amounts of Hyp was analyzed for cross-linking on a Varian HPLC system (with AA911 column, see above) linked to an on-line fluorescence flow monitor (FP-1520, Jasco, Tokyo, Japan) and a liquid scintillation flow monitor (500TR series, Packard Instrument, Meriden, CT, USA). The cross-link precursor aldehydes (i.e., Hylald and Lysald), the major divalent reducible cross-links deH-DHLNL and deH-HLNL were analyzed as their reduced forms, i.e. dihydroxynorleucine (DHNL), hydroxynorleucine (HNL), DHLNL and HLNL, respectively. Hereafter, the reduced forms will be used to indicate these aldehydes and cross-links. The non-reducible cross-links, Lysyl Pyridinoline (LP) and Hydroxylysyl Pyridinoline (HP), were also analyzed simultaneously as previously reported [21]. All cross-links were quantified as moles per mole of collagen (mol/mol of collagen).

2.4. Real-time quantitative RT-PCR

RNA was isolated from left tibia using Trizol reagent (Invitrogen) after flushing bone marrow. cDNA was synthesized using SuperScript II kit (Invitrogen). Taqman primers and probes used in this study were as follows: *Plod1*, Mm01255760_m1 (74 bp); *Plod2*, Mm00478767_m1 (77 bp); *Plod3*, Mm00478798_m1 (62 bp); *Lox*, Mm00495386_m1 (73 bp); *Loxl*1, Mm01145738_m1 (109 bp); *Loxl*2, Mm00804740_m1 (82 bp); *Loxl*3, Mm01184865_m1 (98 bp); *Loxl*4, Mm00446385_m1 (63 bp). Real-time qRT-PCR was performed (ABI 7500 PCR System; Applied Biosystems). Five samples were randomly chosen and all measurements were performed in triplicate. Values were normalized to GAPDH and analyzed using the $2^{-\Delta\Delta Ct}$ method [28].

2.5. Raman microspectroscopy

The Raman system used in this study has been described previously [29]. The right femora (n = 6 each group) were dehydrated in graded ethanol (70%, 80%, 95%, 100%), defatted in Clear-Rite 3 (Richard-Allen Scientific, Kalamazoo, MI, USA), and infiltrated in a liquid methylmethacrylate monomer (Koldmount; Mager Scientific). The bones were embedded in poly-methylmethacrylate (Koldmount Cold Mounting Kit; Mager Scientific). Using a low-speed sectioning saw (Model 650; South Bay Technology, San Clemente, CA, USA) with a diamond wafering blade (Mager Scientific), longitudinal sections (>300 μm in thickness) were made and subsequently transverse sections were cut at the femoral mid-diaphysis (approx. 50% of the total length of femora, Mid) and distal-metaphysis (End). Sections were hand polished using wet silicon carbide abrasive disks to make approximately 300 μm thick sections [30]. For cortical compartments, areas 10 μm from the surface were chosen in the medial quadrant at End and Mid, and both periosteal and endosteal areas were scanned. For trabecular compartments, areas 200–300 μm from the growth plate were chosen (End), and both medial and lateral areas were scanned. At least 3 Raman line spectra were recorded in each location. The periosteal and endosteal data within each of the cortical Mid- and End-diaphysis sections were pooled as no significant differences between location were detected.

At each location, a line-focused 785 nm laser (100 μm in length and 6–8 μm in width) (Invictus, Kaiser Optical Systems, Inc., Ann Arbor, MI, USA) was focused on the specimen through a NIR-optimized 20×/0.75 objective. Raman scatter was collected through the same objective, and delivered to a spectrograph (HoloSpec, Kaiser Optical Systems, Inc.). The Raman scatter was collected on a back-illuminated deep depletion CCD (Newton, Andor Technology, South Windsor, CT, USA). Spectral processing was performed with locally written scripts on Matlab (Math Works, Natick, MA, USA) for spectrograph image curvature, dark-current subtraction, white-light correction [31] and background tissue fluorescence [32]. The data was exported to GRAMS/AI (Thermo Fisher Scientific, Waltham, MA, USA) and spectra were normalized to the height of phosphate ν_1 band (959 cm^{-1}). The number of bands to fit the phosphate ν_1 envelope (approx. 900–990 cm^{-1}) and amide I envelope (approx. 1600–1700 cm^{-1}) was determined by second derivative analysis. The phosphate envelope was fitted to three bands at 918, 946 and 959 cm^{-1}). The amide I envelope was fitted to four bands at 1605, 1635, 1664 and 1685 cm^{-1}. Band areas were determined for select Raman peaks from bone mineral (phosphate, 959 cm^{-1}) and collagen matrix (amide I, 1664 and 1685 cm^{-1}) components. For Raman metrics — the collagen cross-link (maturity) ratio, (1664/1685) indicating cross-link maturation [33], the mineral/matrix ratio (959/[853 + 876)]) describing the amount of mineralization, and crystallinity (inverse of 959 cm^{-1} bandwidth at half the peak intensity) representing mineral crystal size and perfection were calculated [34].

2.6. Nanoindentation

After Raman analysis, the femoral sections (n = 6 each group) were used to measure the material-level mechanical properties by a Nano Indenter II (Nano Instruments, Inc., Oak Ridge, TN, USA). Specimens were examined visually under an optical microscope, and at least five indentations each in the mid-diaphysis (Mid) and distal-metaphysis (End) were made. For cortical compartments, areas 10 μm from surface in the medial quadrant were chosen (End and Mid) and for trabecular compartments, areas 200–300 μm from a growth plate were chosen (End). The indents were made by a diamond Berkovich tip with 30 μm spacing between indents, following a constant displacement rate of 20 nm/s to reach the final displacement of 500 nm. A typical indentation experiment resulted in a loading and unloading force–displacement curve. The elastic moduli E were computed according to Oliver and Pharr's method [35]. $1 / E_r = (1 - \nu^2) / E + (1 - \nu_i^2) / E_i$, where ν is Poisson's ratio of the indented specimen, which was set to be 0.3 assuming the bone to be an isotropic elastic material; ν_i is Poisson's ratio of the indenter tip (equal to 0.07), and E_i is the elastic modulus of the indenter material (equal to 1440 GPa). Reduced elastic modulus E_r was calculated from the slope of a line tangent to the unloading segment of the load–displacement curve at peak indentation load. The hardness values H were determined by the following formula: H = Pmax / A, where Pmax is the peak indentation load and A is the projected contact area at that load. H were computed using the Nano Indenter II® software.

For rib samples (n = 3 each group), a nanoindentation system (950 TI TriboIndenter, Hysitron, Minneapolis, MN) with a 0.5 μm spatial resolution was used. Cortical and trabecular regions of interest were located under the microscope. A diamond tip with Berkovich geometry was used to perform the indents, which consisted of a 10 μN preload, and then a 300 μN/s load rate up to 3000 μN, which was held for 10 s and then unloaded at −300 μN/s for 10 s. Five indents per compartment per sample were made with 15 μm spacing between indents. Load–displacement curves were analyzed to compute the indentation modulus (E) using the Oliver–Pharr method [35]. The five modulus and hardness values were averaged for each sample.

2.7. Micro computed tomography (μCT) evaluation — geometric properties

Left femora (n = 12 for both controls and cKO) were scanned at the proximal metaphysis and the mid-diaphysis using a μCT system (μCT100 Scanco Medical, Bassersdorf, Switzerland). Bones were embedded in agarose to prevent dehydration [36]. Scan settings were voxel size 10 μm, medium resolution, energy 70 kV, intensity 114 μA, 0.5 mm AL filter, and integration time 500 ms. Scans were reoriented using Scanco IPL to match the alignment of each bone in silico with its eventual alignment during mechanical testing, as described [37]. Analysis was performed using the manufacturer's evaluation software. A 1 mm × 1 mm region of the trabecular compartment (50 μm thick) was analyzed beginning 0.2 mm below the growth plate using a fixed global threshold of 25.5% (255 on a grayscale of 0–1000, 554 mg HA/cm^3). Cross-sectional geometry was measured in a 1.5 mm region of the mid-diaphysis in the center

of the 3 mm zone between the inner loading point, and was analyzed using a fixed global threshold of 28% (280 on a grayscale of 0–1000, 628 mg HA/cm^3).

Cortical geometry at the mid-diaphysis was analyzed from thresholded slice images using a custom Matlab script. Measured properties included cortical area, cortical thickness, anterior–posterior (AP) width, medial–lateral (ML) width, bending moment of inertia about the AP and ML axes (I_{AP}, I_{ML}), the distance between the centroid and the anterior surface was measured for use in calculating material level mechanical properties; see Mechanical testing, below.

2.8. Mechanical testing — four point bending

Whole bone (structural level) mechanical testing by four point bending was performed on the left femora ($n = 12$ each) using an Admet eXpert 450 Universal Testing Machine (Norwood, MA, USA) and its manufacturer-provided software for data collection. Whole femora were brought to room temperature prior to testing, hydrated with calcium buffered saline throughout testing, and aligned in the tester with the anterior surface in tension (bending about the medial–lateral axis) and the greater trochanter outside the proximal loading roller (9 mm support span, 3 mm loading span). Bones were loaded to failure at a crosshead displacement rate of 0.025 mm/s. Load and deflection data were recorded for each test and analyzed with the aid of custom Matlab scripts as previously described [30]. During testing, the bone was visually monitored and the point of fracture initiation was noted and measured relative to the proximal end of the bone. Classic beam theory equations were used to calculate estimated stress–strain curves from load–deflection curves using each bone's bending moment of inertia about the testing axis (I_{ML}) and the distance to tensile surface (d from the centroid to the anterior surface) as measured by μCT at the fracture site. Yield was defined using the 0.2% strain offset method [38]. Measures of material-level strength (yield stress, ultimate stress, and failure stress) and structure-level strength (yield force, ultimate force and failure force) are reported, as well as elastic modulus (the slope of the linear portion of the stress–strain curve) and stiffness (the slope of the linear portion of the load–displacement curve) [30].

2.9. Statistical analysis

All results are expressed as mean ± SD. Student's t-tests or Mann–Whitney tests when normality failed were used to compare data between control and cKO mice; $p < 0.05$ indicates significance.

3. Results

3.1. Osteoblast-specific disruption of Bmpr1a leads to a greater level of mature collagen cross-links in femoral bone

To explore the effect of BMPR1A on collagen content and structure, we first measured collagen content (hydroxyproline/dry weight, μm/mg) of whole femora in control and cKO mice (Fig. 1A). There were no significant differences between control (159.6 ± 4.1 μg/mg) and cKO mice (154.9 ± 4.1 μg/mg). Also, there were no significant differences between control and cKO mice regarding Lys hydroxylation (Fig. 1B). These results suggested that BMP signaling through BMPR1A in osteoblasts does not play a critical role in determining the amount of collagen or its Lys hydroxylation.

The concentrations of cross-link precursor aldehydes (DHNL and HNL), reducible divalent cross-links (DHLNL and HLNL) and two nonreducible cross-links (LP and HP) are depicted in Fig. 1C–H. There were no significant changes in aldehydes and reducible cross-links (Fig. 1C, D, E, F) between control and cKO mice. Regarding nonreducible cross-links, however, HP content was significantly larger by 39% in the cKO mice (Fig. 1G, $p < 0.05$), whereas LP did not change between the two groups (Fig. 1H).

The amount and type of collagen cross-links are determined by two groups of enzymes, LOXs and LHs, respectively [20]. To explore the potential effect of BMPR1A signaling on the gene expression of these modifying enzymes, we examined expression of *Plod1*, *2*, and *3* (encoding LH1, 2, 3) and *Lox*, *Loxl1*, *2*, *3* and *4* in the tibia. QRT-PCR results showed *Plod3* and *Loxl4* were significantly up-regulated in the cKO bones compared to controls (Fig. 2, $^*p < 0.05$, $^{**}p < 0.01$).

3.2. Loss of BMPR1A signaling differentially affects the ratio of mature to immature collagen cross-linking in cortical and trabecular compartments of femora

Since μCT results showed a different impact on cortical and trabecular compartments with loss of BMPR1A (Supplementary Tables 1 and 2), we measured cross-linking patterns in cortical and trabecular compartments separately. By employing Raman spectroscopy, the relative % area of the individual underlying bands of Amide I (1664 and 1685 cm^{-1}) was plotted. In the cortical compartments, the cross-linking ratio did not show significant differences between controls and cKO mice (Fig. 3A). In contrast, in the trabecular compartments, the ratio in the cKO mice was significantly increased, by 37%, in the End region (distal-metaphysis of the femora) (Fig. 3B).

3.3. BMPR1A regulates a mineral to matrix ratio in the trabecular compartments of femora

Since the collagen network serves as a template for mineralization, differences in status of collagen cross-links found in the *Bmpr1a* cKO bones may affect the mineralization process. Using Raman spectroscopy, we also examined the relative amounts of mineral and matrix (mineral/matrix ratio, MMR) in femoral cortical and trabecular compartments. There were no significant differences between controls and cKO mice in the femoral cortical compartments (Fig. 3C). However, in trabecular compartments, loss of BMPR1A resulted in significantly larger MMR by 49% (End) in the cKO mice (Fig. 3D). To assess uniformity of the diameter, orientation and distribution of apatite crystals, we examined the crystallinity [34]; there were no significant differences between controls and cKO mice in either the cortical or trabecular compartments (Fig. 3E, F).

3.4. Disruption of Bmpr1a leads to greater intrinsic tissue mechanical properties in the trabecular compartment

To determine whether the alteration in bone composition by loss of BMPR1A signaling influenced femoral biomechanical properties, nanoindentation tests were performed on femoral cortical and trabecular compartments. In the cortical compartment, there were no significant differences in hardness and elastic modulus between cKO and controls (Fig. 4A, C). However, in the trabecular compartment, the cKO bones showed a significant increase in hardness versus the controls (Fig. 4B). Moreover, elastic modulus in the bones from cKO mice increased significantly compared to bones from control mice (Fig. 4D). Both compartments in the ribs from cKO mice showed significant increases in elastic modulus compared to bones from control mice (Fig. 4G, H).

3.5. Disruption of Bmpr1a results in lower femoral bone strength at the structural level due to the decrease in cortical area

To understand the effect of loss of BMPR1A on whole bone strength, we performed four point bending tests at the mid-diaphysis of femoral cortical compartments. Structural-level analyses revealed significantly lower yield force, ultimate force, failure force and stiffness in the mutant bones (Fig. 5A, D). These results demonstrated the cKO bones offered less resistance to external loading. However, no changes were found in deformation and work, including post-yield properties (Fig. 5B, C).

Next, material-level properties were estimated by normalizing structural-level properties by the cross-sectional geometric properties.

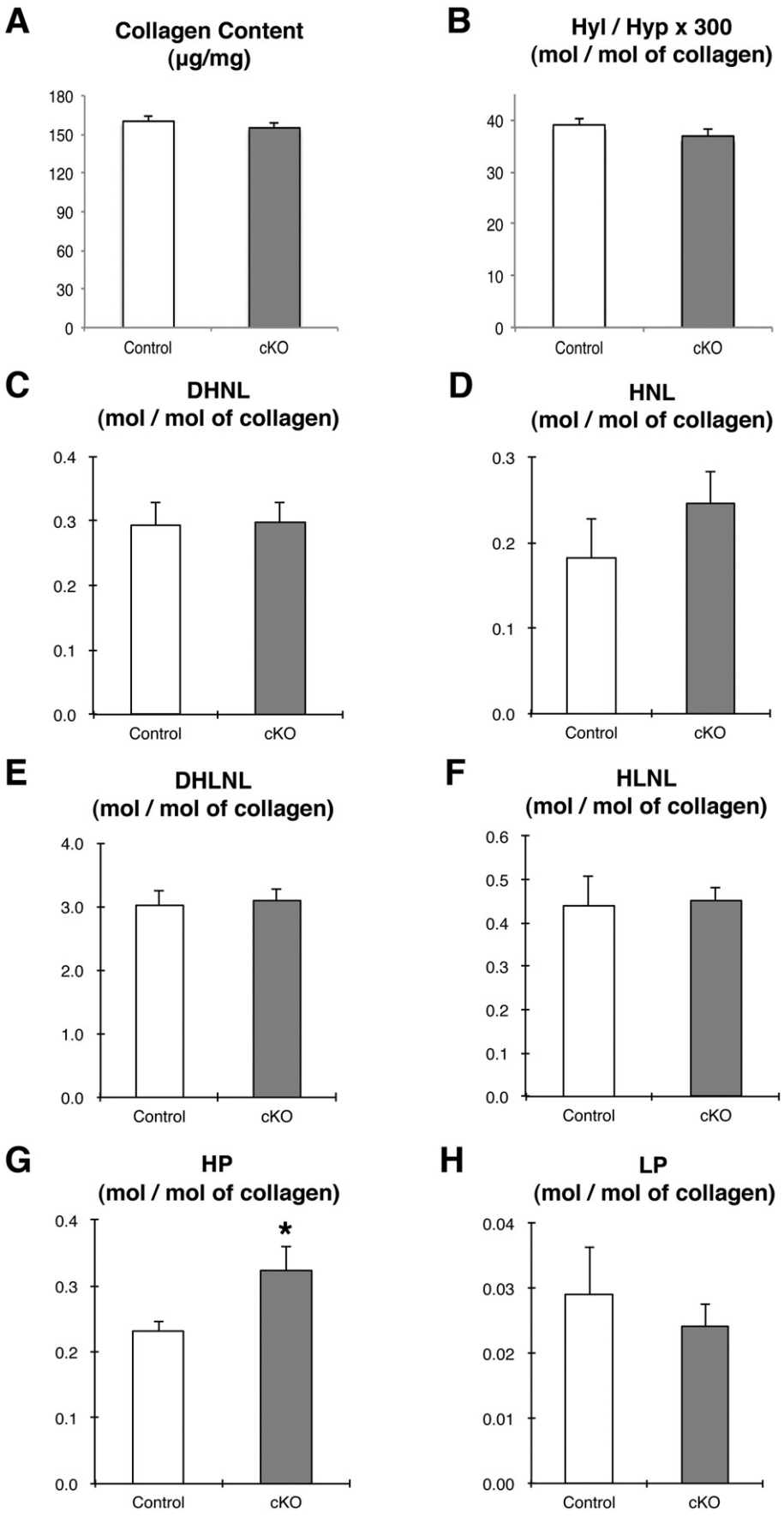
A
Collagen Content
(μg/mg)
180
150
120
90
60
30
0
Control
cKO
B
Hyl / Hyp x 300
(mol / mol of collagen)
40
30
20
10
0
Control
cKO
C
DHNL
(mol / mol of collagen)
0.4
0.3
0.2
0.1
0.0
Control
cKO
D
HNL
(mol / mol of collagen)
0.3
0.2
0.1
0.0
Control
cKO
E
DHLNL
(mol / mol of collagen)
4.0
3.0
2.0
1.0
0.0
Control
cKO
F
HLNL
(mol / mol of collagen)
0.6
0.5
0.4
0.3
0.2
0.1
0.0
Control
cKO
G
HP
(mol / mol of collagen)
*
0.4
0.3
0.2
0.1
0.0
Control
cKO
H
LP
(mol / mol of collagen)
0.04
0.03
0.02
0.01
0.00
Control
cKO

Cortical area and thickness in the cKO bones were significantly lower than controls by 9% ($p < 0.01$) and 7% ($p < 0.01$), respectively (Table 1). The medial-lateral width was also decreased in the cKO mice ($p < 0.01$) (Table 1). However, upon normalization to femoral cross-sectional geometry, the material-level biomechanical properties showed no changes in yield stress, ultimate stress, failure stress or modulus between controls and cKO bones (Fig. 5E, H). These results are in agreement with the nanoindentation results that showed no change in cortical material-level biomechanical properties in the femur (Fig. 4A, C). There were also no significant differences in yield, ultimate, failure and post-yield strains, and toughness (Fig. 5F, G).

4. Discussion

Despite accumulating evidence for the role of BMPs in promoting fracture healing and increasing bone mass, the impact of BMP signaling on bone quality and biomechanical properties under physiological conditions has not been fully elucidated, due to the lack of appropriate genetic animal models. In this study, we deleted *Bmpr1a* in an osteoblast-specific manner in mice when they reached 16 weeks of age, and found that the loss of BMPR1A signaling in osteoblasts changes femoral geometry (Table 1), composition (Figs. 1, 3) and biomechanical properties (Figs. 4, 5). Moreover, we found that the cortical and trabecular compartments are differentially affected in these properties in the cKO mutants. In cortical compartments, the cross-sectional area in the cKO femora is smaller (Table 1), which likely contributes to the decreased structural-level strength (Fig. 5). In the trabecular compartment, the cKO exhibited a greater mature to immature cross-link ratio and mineral matrix ratio (MMR) (Fig. 3), which were associated with greater biomechanical properties (Fig. 4). Taken together, these results indicate that BMPR1A is an important factor under physiological conditions, for maintaining proper geometry within cortical compartments, and bone tissue quality, including collagen cross-linking and mineral deposition within trabecular compartments.

4.1. Loss of BMPR1A in mice leads to greater material-level modulus and hardness in femoral trabecular bone in association with the increased mature cross-links and MMR

Collagen cross-linking plays an important role in bone strength, and is thought to be a determinant of bone quality at the material level [39]. Most likely, increased levels of mature collagen cross-linking are beneficial for bone strength. In our study, we found increased levels of mature cross-links HP in the whole bone (Fig. 1) and an increased mature to immature cross-link ratio in the mutant trabecular compartment, accompanied by significantly increased mineral to matrix ratio (Fig. 3). These alterations in trabecular composition coincide with higher modulus and hardness (Fig. 4). Based on our previous study, where we found greater bone mass in trabecular compartments in cKO femora and no changes in cortical compartments assessed by microCT [8], we believe the change in HPLC data was mainly influenced by trabecular bone, as Raman analyses detected trabecular bone changes in the current study (Fig. 3). Since mouse femora contain more cortical bone than trabecular bone, it is possible that there may be some alterations in cortical bone at levels of scale that were not probed in this study, or at resolutions smaller than what is detectable with the techniques used. However, given the hierarchical approach employed and combination of chemical, spectroscopic, imaging mechanical and molecular assays utilized, the collective data supports the conclusion of trabecular, but not cortical changes.

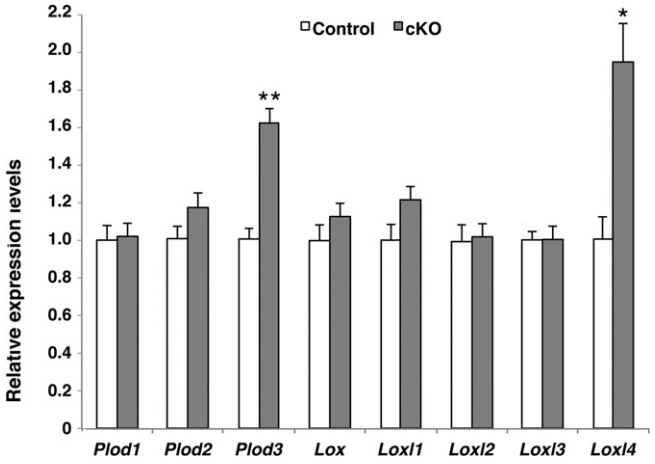

Fig. 2. Loss of BMPR1A increased the expression levels of genes related to collagen post-translational modification. Levels of expression of genes related to collagen cross-linking were measured by QRT-PCR. RNAs were extracted from tibiae. Significant increases in *Plod3* and *Loxl4* expression were detected in cKO mice (mean ± SD, t-test; $^{*}p < 0.05$; $^{**}p < 0.001$; $n = 5$).

Consistent with our results, alfacalcidol treatments improve the strength of fragile bones in rats, which is associated with increases of mature cross-links [40]. Moreover, a reduction of LP and HP cross-links by inhibiting LOX is also associated with reduced strength in the femora of rats [41]. However, association of an increased fracture risk is also reported with increased maturity of collagen cross-links in cortical and trabecular compartments of iliac biopsies [16]. Such discrepancies may be explained by other changes in bone composition, such as increases of crystallinity [16] or increased microheterogeneities in bone matrix composition [42]. Further investigation is necessary to better understand how modifications of cross-linking in the extracellular matrix contribute to biomechanical properties of bone.

The Raman spectroscopic parameters should be interpreted with care. There are two sources of ambiguity in the measurements: the interpretation of components of amide I and the interpretation of mineral to matrix ratio. Since its introduction to bone Fourier transform infrared spectroscopy (FTIR) [33], the intensity ratio of the ~1660 cm^{-1} to ~1690 cm^{-1} components of amide I (largely C═O stretches of the collagen amide backbone) has been used as measure of mature/immature cross-link content. The ratio was soon used in Raman spectroscopy [29], where signal/noise ratios are lower than in FTIR. Although it was recognized by Paschalis et al. to be only an indirect measure of cross-link content, the ratio has since been used in both FTIR and Raman spectroscopies to interpret data from bone in which, for example, pathological cross-links might be formed by incubation with ribose [43] or by administration of ionizing radiation [44]. The ratio as a measurement of cross-link content has come into question because administration of the lysyl oxidase inhibitor beta-aminopropionitrile (BAPN) was found by one group to cause no change in the enzymatic cross-link ratio [45] and by another to cause a change [46]. However, if treatment history and tissue age are carefully controlled for, Raman spectroscopy is able to detect localized matrix differences attributable to crosslinking changes [37].

The Raman microprobe used in this work employs line-focused laser light with the entrance slit of the spectrograph functioning as a spatial filter. This semi-confocal configuration results in partial depolarization of the exciting laser light and the Raman scatter due to the turbidity of the bone tissue [47]. The tissue orientation effects are partially, but not

Fig. 1. Loss of BMPR1A increased non-reduced mature cross-links in collagen. HPLC measurements of collagen content by Hyl/dry ash (A), and the extent of Lys hydroxylation of collagen shown by the ratio of Hyl/Hyp (B), collagen immature cross-links (C, D, E, F), and collagen mature cross-links (G, H) in femora. HP is significantly increased in cKO femur (G), while there are no statistical differences in collagen content (A), the extent of Lys hydroxylation of collagen (B), aldehydes and reducible cross-links (C–F) and LP (H) between bones from control and cKO mice. (mean ± SD, t-test; $^{*}p < 0.05$; $n = 6$ each group). Hyp, Hydroxyproline; Hyl, hydroxylysine; Lys, lysyl; DHNL, droxynorleucine; HNL, hydroxynorleucine; DHLNL, dihydroxylysinonorleucine; HLNL, hydroxylysinonorleucine; LP, Lysyl pyridinoline; HP, Hydroxylysyl pyridinoline.

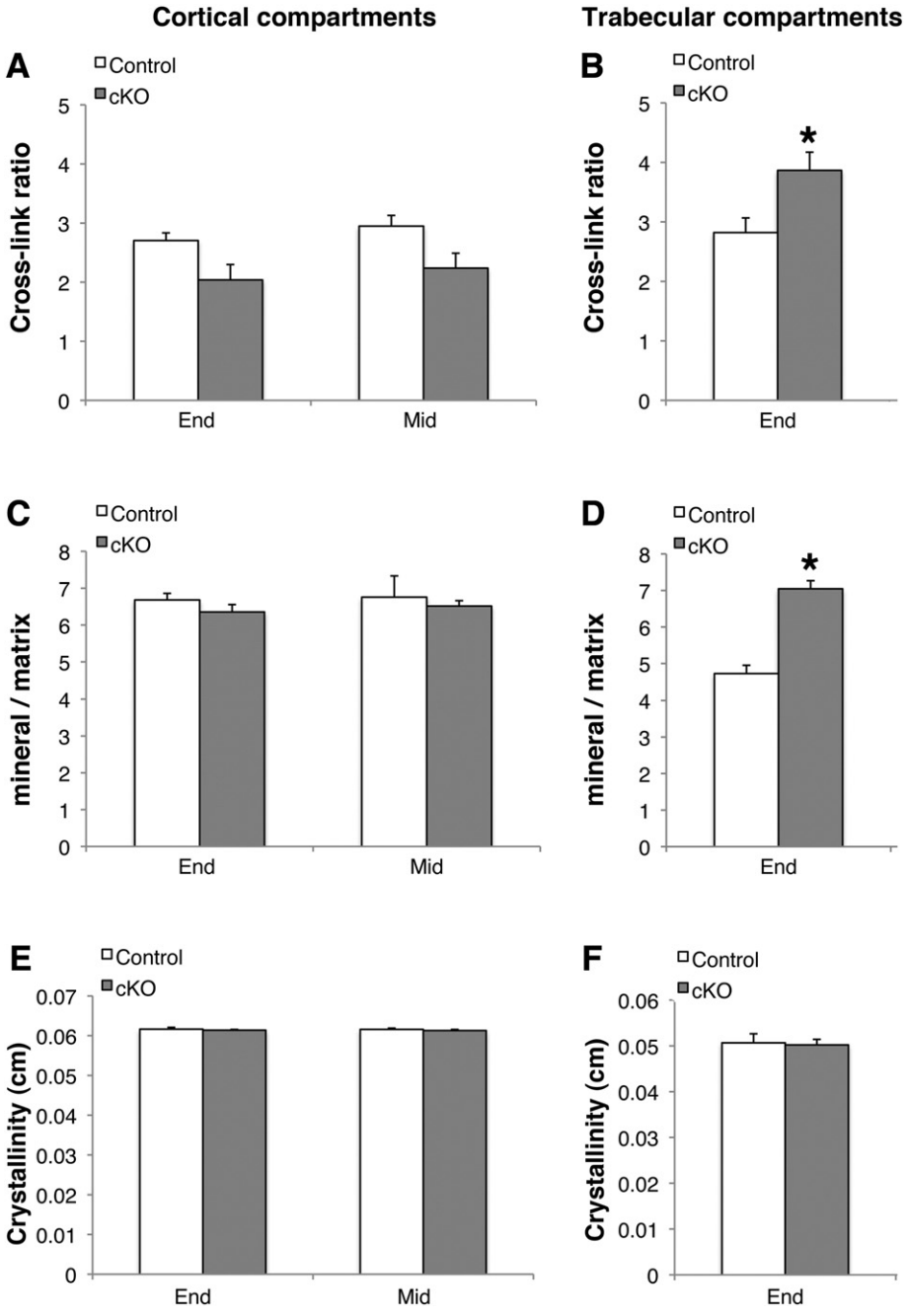

Fig. 3. Loss of BMPR1A increased collagen mature to immature cross-link ratio and mineral to matrix ratio in femoral trabecular bone as measured by Raman spectroscopy. Raman spectroscopy measurements of collagen mature to immature cross-link ratios (A, B), mineral to matrix ratios (MMR) (C, D) and crystallinity (E, F) were evaluated in femora. The distal-metaphysis (End) and the mid-diaphysis (Mid) of femoral cortical compartments and the distal-metaphysis (End) of femoral trabecular bones were examined. Trabecular, but not cortical compartments of cKO femora showed significantly higher mature to immature cross-link ratio and mineral to matrix ratios than in controls. (mean ± SD, t-test; $^{*}p < 0.05$; $n = 6$ each group).

completely eliminated. On the assumption that the relative orientation of phosphate crystallites and collagen fibrils remains constant and independent of changes in cross-link content and amount of mineral, our estimates of mineral/matrix ratio may be a lower limit. However, on the assumption that increasing the cross-link/maturity ratio does not change the relative orientations of collagen carbonyls, the observed collagen cross-link/maturity ratio will be independent of polarization properties. In this study we used a 20×/0.75 objective. Our study of polarization effects in bone spectra obtained with a Raman microprobe using the spectrograph entrance slit as the spatial filter found that the slit functions to partially depolarize the light [47]. The reason is that there is no spatial filtering along the slit length. The order parameter P_2 is reduced from 0.72 to 0.20 when changing from a 40×/0.9 objective to a 20×/0.75. While polarization effects are not completely eliminated, they are greatly attenuated compared to what is obtained with a pinhole spatial filter.

It is not clear if higher levels of HP cross-links are associated with higher MMRs in bones from cKO mice. Mineral characteristics contribute to bone mechanical properties [48], and the greater stiffness and hardness in the mutant trabecular compartments can potentially be explained by the higher MMR. We dehydrated bones for plastic embedding in order to perform Raman and nano-indentation. This processing may have an impact on the results, especially the mechanical characterization. Dehydration increases elastic modulus [49], thus the reported values may be upper limits. However, sample processing would not affect the

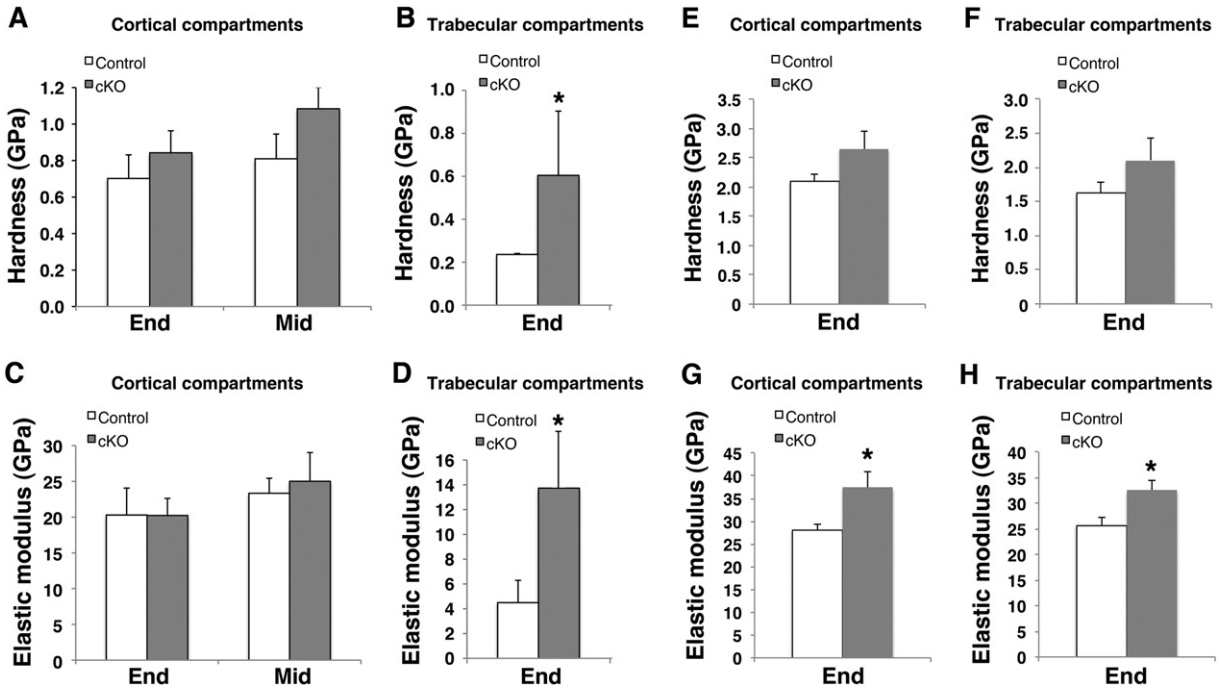

Fig. 4. Loss of BMPR1A increased hardness and elastic modulus in intrinsic trabecular tissues. Nanoindentation measurements of tissue-level biomechanical properties in the distal-metaphysis (End) and mid-diaphysis (Mid) of the cortical compartment (A, C) and End region of the trabecular compartment (B, D) of the femur, and End region of cortical (E, G) and trabecular compartments (F, H) of the rib. Trabecular, but not cortical compartments of cKO femora showed significantly increased hardness and modulus vs. controls, and both compartments of cKO ribs showed significantly increased modulus vs. controls. (mean ± SD, t-test; *$p < 0.05$; n = 6 for femoral controls and cKO, n = 3 for rib controls and cKO).

comparative trends [50]. It is possible that the dehydration/embedding process could influence control and cKO samples differentially due to the differences in quantity and quality of bone composition. However, this scenario is not probable, since much greater changes in composition would be required for similar processing methods to manifest themselves differently.

4.2. The higher levels of mature cross-links in the bones from Bmpr1a cKO mice may be attributed to slower bone turnover

In the bones from *Bmpr1a* cKO mice, the expression of the collagen cross-link associated enzyme genes, including *Plod3* and *Loxl4*, was up-regulated in the tibia (Fig. 2). LP is a trivalent cross-link composed of

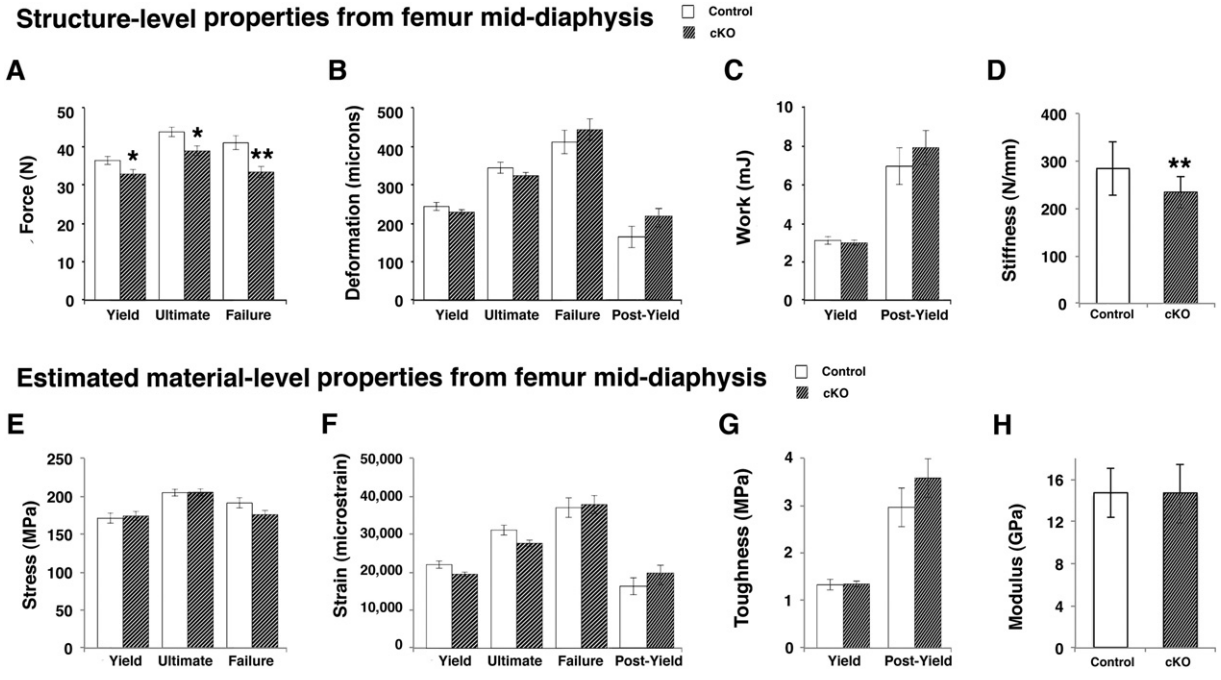

Fig. 5. Loss of BMPR1A undermined the biomechanical properties at the structural-level. Structural-level properties (A, B, C, D) and estimated material-level properties (E, F, G, H) from the mid-diaphysis of cortical femoral compartments. (A) Force (yield, ultimate, and failure force), (B) deformation (yield, ultimate, failure and post-yield deformation, (C) work (yield and post-yield work) and (D) stiffness were evaluated in bones from control and cKO mice. Estimated material-level mechanical properties were calculated by normalizing structural-level properties by cross-sectional geometric properties and shown as (E) stress (yield, ultimate, and failure yield), (F) strain (yield, ultimate, failure and post-yield strain, (G) toughness (yield and post-yield toughness) and (H) modules. (mean ± SD, t-test; *$p < 0.05$; **$p < 0.001$; n = 12 each group).

Table 1
Standard site cross-sectional geometric properties from the mid-diaphysis of femoral cortical bone.

Parameters	Control	cKO
Cortical area (mm^2)	1.26 ± 0.06	1.15 ± 0.1**
Cross-sectional width: A–P (mm)	1.95 ± 0.08	1.82 ± 0.09
Cross-sectional width: M–L (mm)	1.38 ± 0.08	1.33 ± 0.08**
Cross-sectional aspect ratio (A–P width/M–L width)	1.41 ± 0.07	1.37 ± 0.06
A-P moment of inertia (mm^4)	0.22 ± 0.03	0.19 ± 0.04
M-L moment of inertia (mm^4)	0.40 ± 0.04	0.33 ± 0.06
Average cortical thickness (mm)	0.30 ± 0.01	0.28 ± 0.01**
Distance to tensile side (mm)	0.69 ± 0.04	0.66 ± 0.04
Bone length (mm)	17.48 ± 0.46	17.47 ± 0.53

Cortical area, cross-section width (M-L), and average cortical thickness were significantly decreased in bones from cKO vs. control mice. (mean ± SD, t-test; **$p < 0.01$; $n = 12$ each group).
A–P, anterior–posterior; M–L, medial–lateral.

two telopeptidyl Hylalds, and one helical Hyl, thus, each of the three Lys residues involved are hydroxylated. It is possible that upregulation of *Plods* and *Loxs* in the cKO mice may lead to increases in immature crosslinks, yielding a larger number of immature crosslinks. As immature crosslinks convert to mature ones, the number of immature crosslinks decreases and the number of mature crosslinks increases over time, resulting in a larger number of mature crosslinks in the cKO bones. The increased formation of pyridinoline cross-links found in fibrotic disorders patients in association with higher LH levels [51] is consistent with our finding. However, although significant, alterations in *Plod3* and *Loxl4* gene expression are small and it is not clear that crosslink changes found in tibiae can be extrapolated to the femora, where we analyzed collagen crosslinking, since compositional changes in bone are site-specific.

A more plausible explanation for the increase of HP in cKO bones is that bone remodeling in the cKO mice is slower resulting in an increase in mature cross-links. Collagen cross-link formation is tightly regulated by bone turnover rate [52]. As we reported previously, the *Bmpr1a* cKO mice show a slower bone turnover rate in femoral trabecular bones compared to bones from control mice due to the reduction in osteoclastogenesis [7,8]. We observed a reduced bone formation rate in the cKO trabecular compartments [7,8], thus we interpreted that trabecular bone mass is increased due to higher reduction in bone resorption than increase in bone formation. The reduced level of bone turnover in the mutant bones allows the collagen fibrils to mature in the tissue, i.e., once the telopeptideyl lysine and hydroxy-lysine residues are converted to aldehyde by the action of lysyl oxidase, the subsequent divalent and trivalent cross-link reactions are non-enzymatic and spontaneous [53]. This notion is supported by a similar cross-link phenotype seen in toothless (tl/tl) osteopetrotic rats and WBN/Kob diabetic rats in which bone remodeling is diminished [54]. The relatively small changes in collagen cross-links that we observed in bones from cKO mice could be due to the fact that the analysis was done on the whole bone. Since the changes in the Raman spectroscopic parameters are different between trabecular and cortical compartments, cross-link analysis after separation of these compartments may provide more insight into the role of BMPR1A in collagen phenotypes.

4.3. Loss of BMPR1A leads to the reduction in cortical bone strength at the structural level

The strong relationship between cortical area and maximum load suggests that properties of the cortical compartment are important for whole bone strength [18,38]. Loss of BMPR1A decreased cortical area and thickness (Table 1). Larger external bone diameters provide greater strength in bending than smaller external bone diameters, when other structural and compositional parameters are equal (e.g., amount of bone mineral), because resistance to load is primarily a function of cross-sectional geometry of long bones [18,38]. Reduced cortical thickness is associated with wrist fractures in women [55]. Therefore, the lower whole bone strength, including reductions in yield force, ultimate force, failure force, found in the *Bmpr1a* cKO femora (Fig. 5) may be explained by the reduced cortical cross-sectional area. In contrast, we did not find significant differences in deformation, work, strain, and toughness including post-yield properties, in cKO bones compared to controls (Fig. 5). Since modifications in collagen influence post-yield properties, these results are consistent with the lack of significant changes in collagen in cortical bones detected by Raman spectrometry (Fig. 3).

We used mid-diaphyseal μCT images to estimate material properties. The CT site was located at approximately the mid-point (50%) and its 1.5 mm thickness included ~10% of the bone length, thus it covered the span that was 45–55% of bone length. On average, bones fractured at the 60% point of the length, closer to the distal end. Both the CT and fracture sites were within the 4-pt. testing 3 mm inner span.

4.4. Loss of BMPR1A signaling affects femoral cortical and trabecular compartments differently

Femoral trabecular and cortical compartments are affected differently by loss of BMPR1A signaling. In femoral trabecular compartments, *Bmpr1a* deficiency increased BMD, MMR, mature collagen cross-links, and material level biomechanical properties. In cortical compartments, *Bmpr1a* deficiency negatively affected cross-sectional geometries and thus bone strength at the structural level, but material level properties remained unchanged. Interestingly, both cortical and trabecular compartments from cKO ribs showed greater moduli than in control ribs. These different outcomes may be due to differences in anatomical location, origin (lateral mesoderm vs. paraxial mesoderm), or mechanical environment.

Several reports have documented different responses of cortical and trabecular compartments to genetic manipulation, disease and treatments [56,57]. One possible explanation is a difference in bone turnover rate in these two bone types. Generally, the turnover rate in trabecular compartments is higher than that in cortical compartments [58,59]. In our study, we induced Cre activity at 16 weeks by injection of tamoxifen for 5 weeks and harvested bones at 22 weeks, but it may not have been long enough for cortical compartments to make overt changes. Until 16 weeks, when Cre activity is induced by tamoxifen injection, normal bone matrix is formed in both cortical and trabecular compartments. After Cre induction, the *Bmpr1a* deficient osteoblasts change their characteristic to lower bone formation rate [8], reduce supporting function for osteoclastogenesis [8] and increase some of the collagen modifying enzymes (Fig. 2). Thus, bones become a hybrid of normal and newly deposited matrices that have alterations in collagen cross-linking and mineral matrix ratio. Therefore, bones showing a higher turnover (trabecular compartments) should have higher ratio of matrix deposited after induction of Cre recombinase in osteoblasts, leading to the significant alterations in bone quality. An interesting future study will be to treat the mice with tamoxifen for longer periods to investigate alterations in bone quality and biomechanical properties in femoral cortical compartments. However, tamoxifen also influences bone mass. The impact of tamoxifen on tissue-level mechanical properties is poorly understood, and thus we need to be mindful of a possible impact of long-term treatment of tamoxifen. Nonetheless, control mice also received tamoxifen injections, so if there were any influence of tamoxifen on mechanical properties, this is accounted for in the phenotypic comparison of cKO to control mice.

There are interesting contrasts between the results of this study and the phenotype of *Bmp2* cKO mice [10,11]. Removal of *Bmp2* in mesenchymal precursors at embryonic day 10.5 results in smaller cortical compartments and increased fracture risk in adult mice [11]. Osteoblast-specific disruption of *Bmp2* using type 1 collagen-Cre results in reduced trabecular bone volume and mechanical properties at the structural level, but similar cortical thickness compared with controls [10]. There are several possibilities to explain such differences. Functions of ligands

and receptors are not necessarily identical, i.e. a germline mutation in *Bmpr1a* causes embryonic lethality before gastrulation, whereas a mutation in *Bmp2* causes lethality after mesoderm formation [60,61]. Alternatively, it is well accepted that functions of BMP signaling are context dependent, thus, it would not be surprising if consequences of loss of BMP signaling in osteoblasts might be different between embryonic and postnatal stages. In the current study, we induced Cre activity in osteoblasts at 16 weeks after birth while the type 1 collagen-Cre employed to disrupt *Bmp2* is constitutively active from embryonic stages [10]. Interesting future directions would be to further investigate stage-dependent outcomes in bone quality and biomechanical properties by alternating levels of BMP signaling. Nonetheless, we think the precise regulation of BMP signaling through BMPR1A may have a clinical advantage to restore tissue quality and strengthen bone in patients with high risk of bone fracture. Suppression of BMPR1A signaling by administration of a soluble form of BMPR1A prevents ovariectomy-induced bone loss and improves bone strength [13]. Therefore, these innovative interventions would be worth considering in order to improve bone quality to reduce risk of fracture.

5. Conclusions

In this study, we have shown that loss of BMP signaling through BMPR1A in osteoblasts results in increased levels of mature collagen cross-links and mineral to matrix ratio in trabecular compartments of femora. These compositional changes were associated with greater tissue-level biomechanical properties in trabecular bone, including hardness and elastic modulus. Loss of BMPR1A differentially affected the cortical compartment of femora to reduce cross-sectional area, likely leading to the decreased structure-level strength. These results indicate that BMP signaling mediated by BMPR1A in osteoblasts is an important factor for maintaining normal bone tissue quality that affect biomechanical properties.

Disclosure page

All authors state that they have no conflicts of interest.

Acknowledgment

We thank Drs. Hank Kronenberg and Tatsuya Kobayashi for providing *Col1CreERTM* mice; Dr. Gurjit Mandair for advice on Raman analyses, Drs. Kenneth Kozloff and Joseph Perosky for advice on nanoindentation; Ms. Toni Ward, Ms. Kelly McCann and Ms. Xixi Wang for maintaining mouse colonies; Ms. Caitlyn Molloy for excellent technical assistance; and Dr. Judith Connett for critical reading and editing of this manuscript. This study is supported by the National Institutes of Health (R01DE020843 and ES071003-11 to YM, R01ARAR047969 to MDM) and Department of Defense (DOD W81XWH-12-2-0008 to MXP). The μCT core at the School of Dentistry, University of Michigan is funded in part by NIH/NCRR S10RR026475-01.

Authors' roles: Study design: YZ, NK and YM. Materials to generate: YZ, NK, GJS, MKR, YM. Study conduct: Data collection: Data analysis: YZ, HZ. μCT: YZ, ML, DHK. 4-point bending test: Data collection; MTa, Data analysis; EGM, DHK. Raman analyses: MR, PZ and MDM. Collagen analyses: MTe and MY. Nanoindentation: YZ, GR, ZZ, HZ, MXP, DHK. Data interpretation: YZ, GR, HZ, DHK and YM. Drafting manuscript: YZ, HZ, DHK and YM. Approving final version of manuscript: YZ, NK, EGM, MTa, GR, HZ, MR, PZ, MTe, ZZ, ML, GJS, MKR, MY, PXM, MDM, DHK, and YM. YZ and YM take responsibility for the integrity of the data analysis.

Appendix A. Supplementary data

Supplementary data to this article can be found online at http://dx.doi.org/10.1016/j.bone.2016.04.022.

References

[1] M. Urist, Bone: formation by autoinduction, Science 893-9 (1965).
[2] J.W. Lowery, D.Pazin, G. Intini, S. Kokabu, V. Chappuis, L.P. Capelo, et al., The role of BMP2 signaling in the skeleton. Crit. Rev. Eukaryot. Gene Expr. 21: 177–85.
[3] N.Y. Yu, A. Schindeler, M. Tagil, A.J. Ruys, D.G. Little, Use of BMPs and bisphosphonates in improving bone fracture healing, Front. Biosci. (Elite Ed.) 4 (2012) 2647–2653.
[4] S. Kishigami, Y. Mishina, BMP signaling and early embryonic patterning, Cytokine Growth Factor Rev. 16 (2005) 265–278.
[5] N. Kamiya, Y. Mishina, New insights on the roles of BMP signaling in bone—a review of recent mouse genetic studies, Biofactors 37 (2011) 75–82.
[6] Y. Mishina, M.W. Starbuck, M.A. Gentile, T. Fukuda, V. Kasparcova, J.G. Seedor, et al., Bone morphogenetic protein type IA receptor signaling regulates postnatal osteoblast function and bone remodeling, J. Biol. Chem. 279 (2004) 27560–27566.
[7] N. Kamiya, L. Ye, T. Kobayashi, Y. Mochida, M. Yamauchi, H.M. Kronenberg, et al., BMP signaling negatively regulates bone mass through sclerostin by inhibiting the canonical Wnt pathway, Development 135 (2008) 3801–3811.
[8] N. Kamiya, L. Ye, T. Kobayashi, D.J. Lucas, Y. Mochida, M. Yamauchi, et al., Disruption of BMP signaling in osteoblasts through type IA receptor (BMPRIA) increases bone mass, J. Bone Miner. Res. 23 (2008) 2007–2017.
[9] N. Kamiya, T. Kobayashi, Y. Mochida, P.B. Yu, M. Yamauchi, H.M. Kronenberg, et al., Wnt inhibitors Dkk1 and Sost are downstream targets of BMP signaling through the type IA receptor (BMPRIA) in osteoblasts, J. Bone Miner. Res. 25 (2010) 200–210.
[10] W. Yang, D. Guo, M.A. Harris, Y. Cui, J. Gluhak-Heinrich, J. Wu, et al., Bmp2 in osteoblasts of periosteum and trabecular bone links bone formation to vascularization and mesenchymal stem cells, J. Cell Sci. 126 (2013) 4085–4098.
[11] K. Tsuji, A. Bandyopadhyay, B.D. Harfe, K. Cox, S. Kakar, L. Gerstenfeld, et al., BMP2 activity, although dispensable for bone formation, is required for the initiation of fracture healing, Nat. Genet. 38 (2006) 1424–1429.
[12] N. Kamiya, V.M. Kaartinen, Y. Mishina, Loss-of-function of ACVR1 in osteoblasts increases bone mass and activates canonical Wnt signaling through suppression of Wnt inhibitors SOST and DKK1, Biochem. Biophys. Res. Commun. 414 (2011) 326–330.
[13] M. Baud'huin, N. Solban, M. Cornwall-Brady, D. Sako, Y. Kawamoto, K. Liharska, et al., A soluble bone morphogenetic protein type IA receptor increases bone mass and bone strength, Proc. Natl. Acad. Sci. U. S. A. 109 (2012) 12207–12212.
[14] M. Okamoto, J. Murai, H. Yoshikawa, N. Tsumaki, Bone morphogenetic proteins in bone stimulate osteoclasts and osteoblasts during bone development, J. Bone Miner. Res. 21 (2006) 1022–1033.
[15] X. Banse, When density fails to predict bone strength, Acta Orthop. Scand. Suppl. 73 (2002) 1–57.
[16] S. Gourion-Arsiquaud, D. Faibish, E. Myers, L. Spevak, J. Compston, A. Hodsman, et al., Use of FTIR spectroscopic imaging to identify parameters associated with fragility fracture, J. Bone Miner. Res. 24 (2009) 1565–1571.
[17] M.L. Bouxsein, Bone quality: where do we go from here? Osteoporos. Int. 14 (Suppl. 5) (2003) S118–S127.
[18] D.T. Reilly, A.H. Burstein, The elastic and ultimate properties of compact bone tissue, J. Biomech. 8 (1975) 393–405.
[19] D.R. Eyre, M.A. Weis, Bone collagen: new clues to its mineralization mechanism from recessive osteogenesis imperfecta, Calcif. Tissue Int. 93 (2013) 338–347.
[20] M. Yamauchi, M. Sricholpech, Lysine post-translational modifications of collagen, Essays Biochem. 52 (2012) 113–133.
[21] M. Sricholpech, I. Perdivara, M. Yokoyama, H. Nagaoka, M. Terajima, K.B. Tomer, et al., Lysyl hydroxylase 3-mediated glucosylation in type I collagen: molecular loci and biological significance, J. Biol. Chem. 287 (2012) 22998–23009.
[22] S. Hayashi, A.P. McMahon, Efficient recombination in diverse tissues by a tamoxifen-inducible form of Cre: a tool for temporally regulated gene activation/inactivation in the mouse, Dev. Biol. 244 (2002) 305–318.
[23] J. Rossert, H. Eberspaecher, B. de Crombrugghe, Separate cis-acting DNA elements of the mouse pro-alpha 1(I) collagen promoter direct expression of reporter genes to different type I collagen-producing cells in transgenic mice, J. Cell Biol. 129 (1995) 1421–1432.
[24] Y. Mishina, M.C. Hanks, S. Miura, M.D. Tallquist, R.R. Behringer, Generation of Bmpr/Alk3 conditional knockout mice, Genesis 32 (2002) 69–72.
[25] M. Yamauchi, M. Shiiba, Lysine hydroxylation and cross-linking of collagen, Methods Mol. Biol. 446 (2008) 95–108.
[26] M. Katafuchi, T. Matsuura, P. Atsawasuwan, H. Sato, M. Yamauchi, Biochemical characterization of collagen in alveolar mucosa and attached gingiva of pig, Connect. Tissue Res. 48 (2007) 85–92.
[27] M. Yamauchi, E.P. Katz, G.L. Mechanic, Intermolecular cross-linking and stereospecific molecular packing in type I collagen fibrils of the periodontal ligament, Biochemistry 25 (1986) 4907–4913.
[28] K.J. Livak, T.D. Schmittgen, Analysis of relative gene expression data using real-time quantitative PCR and the 2(−Delta Delta C(T)) method, Methods 25 (2001) 402–408.
[29] A. Carden, R.M. Rajachar, M.D. Morris, D.H. Kohn, Ultrastructural changes accompanying the mechanical deformation of bone tissue: a Raman imaging study, Calcif. Tissue Int. 72 (2003) 166–175.
[30] J.M. Wallace, K. Golcuk, M.D. Morris, D.H. Kohn, Inbred strain-specific response to biglycan deficiency in the cortical bone of C57BL6/129 and C3H/He mice, J. Bone Miner. Res. 24 (2009) 1002–1012.
[31] A. Cao, A.K. Pandya, G.K. Serhatkulu, R.E. Weber, H. Dai, J.S. Thakur, et al., A robust method for automated background subtraction of tissue fluorescence, J. Raoan. Spectrosc. 38 (2007) 1199–1205.
[32] F.W. Esmonde-White, K.A. Esmonde-White, M.D. Morris, Minor distortions with major consequences: correcting distortions in imaging spectrographs, Appl. Spectrosc. 65 (2011) 85–98.

[33] E.P. Paschalis, K. Verdelis, S.B. Doty, A.L. Boskey, R. Mendelsohn, M. Yamauchi, Spectroscopic characterization of collagen cross-links in bone, J. Bone Miner. Res. 16 (2001) 1821–1828.
[34] J.J. Freeman, B. Wopenka, M.J. Silva, J.D. Pasteris, Raman spectroscopic detection of changes in bioapatite in mouse femora as a function of age and in vitro fluoride treatment, Calcif. Tissue Int. 68 (2001) 156–162.
[35] W.C. Oliver, G.M. Pharr, An improved technique for determining hardness and elastic modulus using load and displacement sensing indentation experiments, J. Mater. Res. 7 (1992) 1564–1583.
[36] H.F. Luderer, S. Bai, G.D. Longmore, The LIM protein LIMD1 influences osteoblast differentiation and function, Exp. Cell Res. 314 (2008) 2884–2894.
[37] E.M. McNerny, B. Gong, M.D. Morris, D.H. Kohn, Bone fracture toughness and strength correlate with collagen cross-link maturity in a dose-controlled lathyrism mouse model, J. Bone Miner. Res. 30 (2015) 455–464.
[38] C.H. Turner, D.B. Burr, Basic biomechanical measurements of bone: a tutorial, Bone 14 (1993) 595–608.
[39] E.P. Paschalis, E. Shane, G. Lyritis, G. Skarantavos, R. Mendelsohn, A.L. Boskey, Bone fragility and collagen cross-links, J. Bone Miner. Res. 19 (2004) 2000–2004.
[40] M. Saito, K. Marumo, C. Ushiku, S. Kato, S. Sakai, N. Hayakawa, et al., Effects of alfacalcidol on mechanical properties and collagen cross-links of the femoral diaphysis in glucocorticoid-treated rats, Calcif. Tissue Int. 88 (2011) 314–324.
[41] H. Oxlund, M. Barckman, G. Ortoft, T.T. Andreassen, Reduced concentrations of collagen cross-links are associated with reduced strength of bone, Bone 17 (1995) 365S–371S.
[42] S. Gourion-Arsiquaud, L. Lukashova, J. Power, N. Loveridge, J. Reeve, A.L. Boskey, Fourier transform infrared imaging of femoral neck bone: reduced heterogeneity of mineral-to-matrix and carbonate-to-phosphate and more variable crystallinity in treatment-naive fracture cases compared with fracture-free controls, J. Bone Miner. Res. 28 (2013) 150–161.
[43] Y. Iwasaki, J.J. Kazama, H. Yamato, M. Fukagawa, Changes in chemical composition of cortical bone associated with bone fragility in rat model with chronic kidney disease, Bone 48 (2011) 1260–1267.
[44] C.N. Tchanque-Fossuo, B. Gong, B. Poushanchi, A. Donneys, D. Sarhaddi, K.K. Gallagher, et al., Raman spectroscopy demonstrates Amifostine induced preservation of bone mineralization patterns in the irradiated murine mandible, Bone 52 (2013) 712–717.
[45] D. Farlay, M.E. Duclos, E. Gineyts, C. Bertholon, S. Viguet-Carrin, J. Nallala, et al., The ratio 1660/1690 cm(−1) measured by infrared microspectroscopy is not specific of enzymatic collagen cross-links in bone tissue, PLoS One 6 (2011), e28736.
[46] E.P. Paschalis, D.N. Tatakis, S. Robins, P. Fratzl, I. Manjubala, R. Zoehrer, et al., Lathyrism-induced alterations in collagen cross-links influence the mechanical properties of bone material without affecting the mineral, Bone 49 (2011) 1232–1241.
[47] M. Raghavan, N.D. Sahar, R.H. Wilson, M.A. Mycek, N. Pleshko, D.H. Kohn, et al., Quantitative polarized Raman spectroscopy in highly turbid bone tissue, J. Biomed. Opt. 15 (2010) 037001.
[48] J.F. Veenland, T.M. Link, W. Konermann, N. Meier, J.L. Grashuis, E.S. Gelsema, Unraveling the role of structure and density in determining vertebral bone strength, Calcif. Tissue Int. 61 (1997) 474–479.
[49] J.Y. Rho, G.M. Pharr, Effects of drying on the mechanical properties of bovine femur measured by nanoindentation, J. Mater. Sci. Mater. Med. 10 (1999) 485–488.
[50] S. Hengsberger, A. Kulik, P. Zysset, Nanoindentation discriminates the elastic properties of individual human bone lamellae under dry and physiological conditions, Bone 30 (2002) 178–184.
[51] A.J. van der Slot, A.M. Zuurmond, A.J. van den Bogaerdt, M.M. Ulrich, E. Middelkoop, W. Boers, et al., Increased formation of pyridinoline cross-links due to higher telopeptide lysyl hydroxylase levels is a general fibrotic phenomenon, Matrix Biol. 23 (2004) 251–257.
[52] E. Seeman, P.D. Delmas, Bone quality—the material and structural basis of bone strength and fragility, N. Engl. J. Med. 354 (2006) 2250–2261.
[53] M. Yamauchi, Collagen: the major matrix molecule in mineralized tissues, in: J.B. Anderson, S.C. Garner (Eds.), Calcium and Phophorus in Health and Disease, CRC, Boca Raton, FL 1995, pp. 127–145.
[54] A. Wojtowicz, A. Dziedzic-Goclawska, A. Kaminski, W. Stachowicz, K. Wojtowicz, S.C. Marks Jr., et al., Alteration of mineral crystallinity and collagen cross-linking of bones in osteopetrotic toothless (tl/tl) rats and their improvement after treatment with colony stimulating factor-1, Bone 20 (1997) 127–132.
[55] E. Sornay-Rendu, S. Boutroy, F. Munoz, P.D. Delmas, Alterations of cortical and trabecular architecture are associated with fractures in postmenopausal women, partially independent of decreased BMD measured by DXA: the OFELY study, J. Bone Miner. Res. 22 (2007) 425–433.
[56] S. Yakar, C.J. Rosen, M.L. Bouxsein, H. Sun, W. Mejia, Y. Kawashima, et al., Serum complexes of insulin-like growth factor-1 modulate skeletal integrity and carbohydrate metabolism, FASEB J. 23 (2009) 709–719.
[57] M. Michalsky, K. Norris-Suarez, P. Bettica, A. Pecile, L. Moro, Rat cortical and trabecular bone collagen glycosylation are differently influenced by ovariectomy, Biochem. Biophys. Res. Commun. 192 (1993) 1281–1288.
[58] H. Otomo, A. Sakai, S. Ikeda, S. Tanaka, M. Ito, R.J. Phipps, et al., Regulation of mineral-to-matrix ratio of lumbar trabecular bone in ovariectomized rats treated with risedronate in combination with or without vitamin K2, J. Bone Miner. Metab. 22 (2004) 404–414.
[59] P. Magnusson, L. Larsson, M. Magnusson, M.W. Davie, C.A. Sharp, Isoforms of bone alkaline phosphatase: characterization and origin in human trabecular and cortical bone, J. Bone Miner. Res. 14 (1999) 1926–1933.
[60] Y. Mishina, A. Suzuki, N. Ueno, R.R. Behringer, Bmpr encodes a type I bone morphogenetic protein receptor that is essential for gastrulation during mouse embryogenesis, Genes Dev. 9 (1995) 3027–3037.
[61] H. Zhang, A. Bradley, Mice deficient for BMP2 are nonviable and have defects in amnion/chorion and cardiac development, Development 122 (1996) 2977–2986.